Int J Adv Manuf Technol (2017) 90:561–574
DOI 10.1007/s00170-016-9366-x

ORIGINAL ARTICLE

Defects monitoring of laser metal deposition using acoustic emission sensor

Haythem Gaja[1] · **Frank Liou**[1]

Received: 16 May 2016 / Accepted: 19 August 2016 / Published online: 3 September 2016

Abstract Laser metal deposition (LMD) is an advanced additive manufacturing (AM) process used to build or repair metal parts layer by layer for a range of different applications. Any presence of deposition defects in the part produced causes change in the mechanical properties and might cause failure to the part. Corrective remedies to fix these defects will increase the machining time and costs. In this work, a novel defects monitoring system was proposed to detect and classify defects in real time using an acoustic emission (AE) sensor and an unsupervised pattern recognition analysis (K-means clustering) in conjunction with a principal component analysis (PCA). A time domain and frequency domain relevant descriptors were used in the classification process to improve the characterization of the defects sources. The methodology was found to be efficient in distinguishing two types of signals that represent two kinds of defects, which are cracks and porosities. A cluster analysis of AE data is achieved and the resulting clusters correlated with the defects sources during laser metal deposition. It was found that cracks and pores that occur during LMD can be detected using an AE sensor. Pores produce acoustic emission events with high energy, shorter decay time, and less amplitude when compared to cracks. Specifically, the signal energy is a crucial feature in identifying the AE defect source mechanisms. The frequency is not significant; it has a little contribution to the classification solution.

Keywords Laser metal deposition · Deposition defects · Acoustic emission · Clustering analysis · Principal component analysis

1 Introduction

In general, additive manufacturing is extensively used even though monitoring and detection of defects during AM still require a better understanding. One of the difficulties in using an adaptive control and LMD monitoring system is the accurate detection of defects as being formed during the metal deposition. The purpose of monitoring laser metal deposition process is to prevent and detect damage of produced part for any deposition path and part design. In the LMD process, particular changes in the acoustic emission signal indicate the present of defects, these changes must be carefully considered to ensure the effectiveness of the control system. AE has the advantage of real-time, continuous monitoring of LMD. The central goal of such a system is to indicate the occurrence of defects events, but classifying the type of defect is also necessary for the better use of the system and suggestion of corrective remedies.

Laser metal deposition (LMD) is one of the powder-based laser deposition additive manufacturing techniques such as laser cladding (LC) [2, 3], laser direct casting (LDC) [4, 5], direct metal deposition (DLD) [6], directed light fabrication (DLF) [7–9], laser forming (Lasform) [10], shape deposition manufacturing (SDM) [11], laser engineered net shaping (LENS) [12, 13], free form laser consolidation (LC) [14, 15], and many others. The main process parameters of LMD—laser power, travel velocity, and powder flow rate—control the geometry accuracy and the mechanical properties of the finished part by

✉ Haythem Gaja
hmgkc7@mst.edu

[1] Department of Mechanical and Aerospace Engineering, Missouri University of Science and Technology, Rolla, MO 65409, USA

determining the size of the molten pool, the part deformation, and the microstructure of the deposited layers. They affect the temperature profile and cooling rate in the molten pool, as well as the thermal cycles at each location of the fabricated part [1].

The acoustic emission sensor is a piezoelectric transducer that generates an electrical charge as a response to the elastic waves emitted from sources inside a material as a result of the sudden release of energy. The AE technique is one of the most powerful monitoring technologies; it has been used for monitoring in many manufacturing processes such as cutting operations [16–18] and the welding processes. Jolly [1] monitored the crack growth in stainless steel welds. It was found that a maximum AE rate is directly related to the number of cracks in the weld defect zone. This work is considered to be the first most significant milestone in the application of the AE technique for monitoring the welding process [2]. A.S.Sun. Rostek [3] in 1990 used computer-aided acoustic pattern recognition to demonstrate the monitoring capabilities of acoustic signals. Duley and Mao [4] studied the laser welding process of aluminum 1100 using acoustic emission. They found that a keyhole could be identified by specific AE frequency components and correlate the AE with laser penetration and surface condition. Grad et al. [5] in 1996 developed a monitoring method using different statistical parameters to assess process stability.

Bohemen [6] demonstrated that martensite formation during gas tungsten arc (GTA) welding of steel 42CrMo4 can be monitored by means of AE. It was shown that a particular relation exists between the root mean square (RMS) value of the measured AE and the volume rate of the martensite formation during GTA welding. Recently, Grad et al. [7] examined the acoustic waves generated during short circuit gas metal arc welding process. It was found that the acoustic method can be used to assess welding process stability and to detect the severe discrepancies in arc behavior.

Yang [9] recently used an acoustic emission (AE) sensor to identify damage detection in metallic materials. Results suggested a strong correlation between AE features, i.e., RMS value of the reconstructed acoustic emission signal, and surface burn, residual stress value, as well as hardness of steels. Diego-Vallejo [8] in his work found that the focus position, as an important parameter in the laser material interactions, changes the dynamics and geometric profile of the machined surface and also the statistical properties of measured AE signal.

However, more research needs to be done regarding using the acoustic emission sensor in monitoring laser metal deposition. In this paper, the defects type distinguishing of the LMD and its corresponding key features are investigated by clustering the AE signals. The acoustic emission (AE) technique is suitable to examine the defects sources during LMD because it contains rich defect-related information such as crack and pore formation, nucleation, and propagation. Information on defects development is difficult to obtain by only using the AE waveform in a time-space, as a non-stationary process, thus other features such as amplitude, energy, rise time, count, and frequency are extracted to qualitatively analyze defects mechanisms.

The purpose of the present work is first to detect laser metal deposition defects as formed layer by layer to take the necessary correction action such as machining and remitting, and second to develop a reliable method of analysis of AE data during LMD when several AE sources are activated to categorize the defects into clusters based on the defect type.

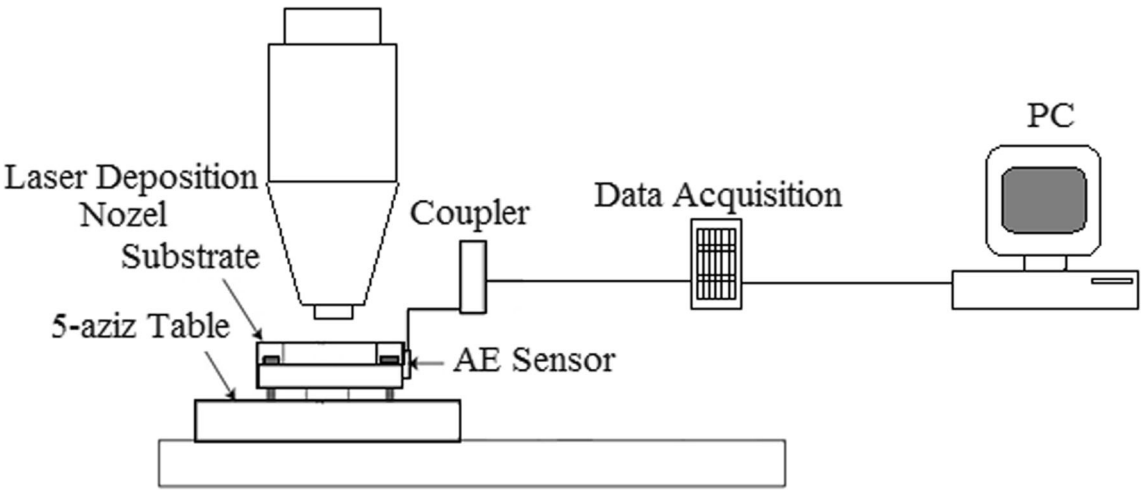

Fig. 1 Experimental setup showing the LMD system and AE data acquisition system

Table 1 The composition and thermal properties of titanium and tool steel metallic powders (mass %)

	Ti-6Al-4V	H13
Iron, Fe	<0.25	Balance
Chromium, Cr	–	4.75–5.5
Molybdenum, Mo	–	1.1–1.75
Silicon, Si	–	0.80–1.20
Vanadium, V	3.50–4.50	0.80–1.20
Carbon, C	<0.08	0.32–0.45
Nickel, Ni	–	0.3
Manganese, Mn	–	0.20–0.50
Titanium, Ti	Balance	–
Aluminum, Al	5.50–6.50	–
Thermal expansion ($°K^{-1}$)	11×10^{-6} to 15×10^{-6}	13×10^{-6} to 16×10^{-6}
Thermal conductivity (W/mK)	8	28.6

2 Experiments and data collection

Figure 1 shows a schematic diagram of the experimental set-up. The YAG laser was attached to a five-axis vertical computer numerical control machine that is used for post-process machining after LMD. Picoscope 2205A works as a dual-channel oscilloscope to capture the AE signal and stream it to a computer for further analysis; the oscilloscope measures the change in the acoustic emission signal over time and helps in displaying the signal as a waveform in a graph. An acoustic emission sensor (Kistler 8152B211) captured a high-frequency signal. The bandwidth of the AE sensor was 100 to 1000 kHz. The raw signals were first fed through the data acquisition system and then processed and recorded using Matlab software.

A powder feeder system is used to deliver the atomized powder to the melt pool by means of argon gas. Argon gas is also used as a shielding gas; it flows through channels in the nozzle of laser deposition head to reduce oxidation of the deposit. During the laser metal deposition process, porosities and cracks can be formed as a result of lack of fusion, shield gas trapping, and the difference in thermal coefficients of the deposited material and the substrate. The acoustic emission signal was recorded during a laser deposition process in an oxidized environment and contaminated powder to induce pores and cracks as a result of thermal coefficient difference. The material of the substrate was tool steel. Cracks and porosities were simulated by mixing the mainly Ti-6Al-4V powder with H13 tool steel powder. Table 1 shows the chemical composition and the thermal properties of both powders. The two powder particles as illustrated in Fig. 2 are non-uniform in shape and size and may contain internal voids which can cause deposition defects when they are mixed. Table 1 displays the chemical composition and the thermal properties of both powders.

Figure 3 illustrates the main steps in the developed procedure which is used to analyze the AE data. A layer is created by injecting the metal powder into a laser beam which is used to melt the surface of a substrate and create a small molten pool and generate a deposit. The AE sensor is attached to a substrate to transform the energy released by the laser deposition into acoustic emission signal. The total length of the deposition is 15 mm and was performed with standard parameters for depositing titanium powder as shown in Table 2.

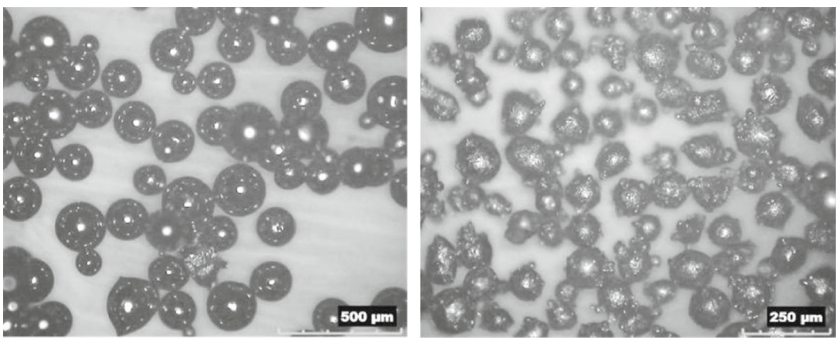

(a) Ti-6Al-4V Metal Powder (b) H13 Metal Powder

Fig. 2 **a**, **b** Optical image of the metal powders used in the deposition process

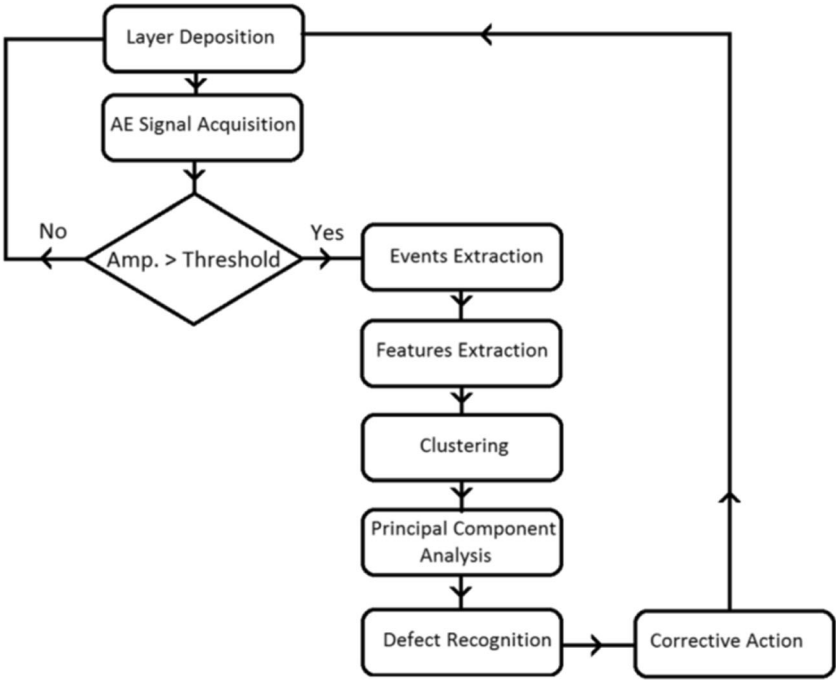

Fig. 3 Step-by-step operations used to perform the acoustic emission analyses

Table 2 Laser metal deposition process parameters

Parameter	Value
Laser power	1000 W
Powder feed rate	10 g/min
Table velocity	300 mm/min
Length of track	15 mm
Layer thickness	About 0.5 mm
Layer width	About 2.5 mm

The formation of porosities and cracks leads to generate an acoustic emission signal, an elastic wave that travels from the source toward a sensor, moving through the substrate until it arrives at the acoustic emission sensor. In response, the sensor produces an electrical signal, which is passed to the electronic equipment for further processing and detection of a defect. Since the LMD is an additive process and it deposits metals layer by layer, the AE signal was recorded for each layer and analyzed to extract any useful information from the AE events.

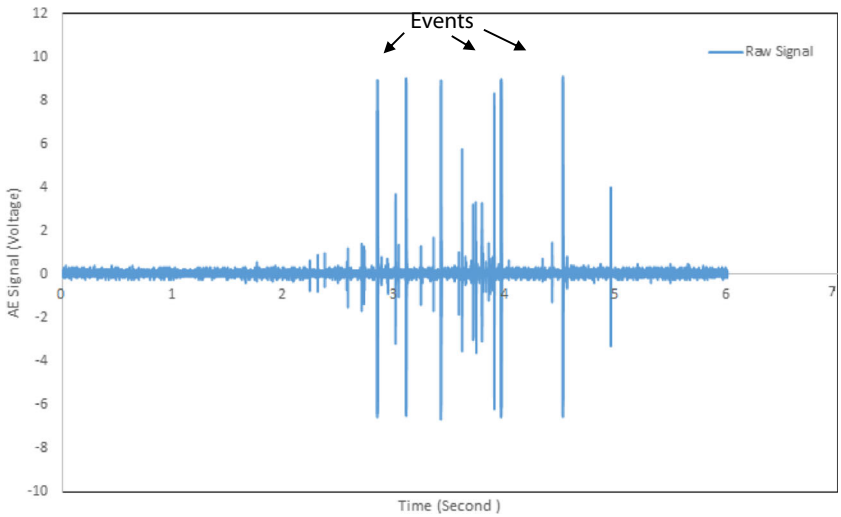

Fig. 4 AE raw signal acquired during the LMD process

Table 3 Time domain and frequency domain AE signal features

Feature	Definition
Peak amplitude	It is the greatest measured voltage in an AE event
Kurtosis	It is a measure of whether the data of an AE event are peaked or flat compared to a normal distribution. $\text{Kurtosis} = \sum_{i=1}^{N} \left(x_i - \bar{x}\right) \frac{2/N}{\sigma^4 - 3}$ (1) where N is the number of samples (x_i) in an AE signal, σ is the standard deviation, and x is the mean.
Energy	Since the domain of the AE event signal is discrete, the energy of the signal is given by $\text{Energy} = \sum_{i=1}^{N} (x_i)^2$ (2)
Number of counts	It is the number of pulses emitted by the AE event.
Duration	It is the time difference between the first and last threshold crossings.
Rise time	It is the time interval between the first threshold crossing and the AE event peak.
Peak amplitude frequency	It is a characterization of the magnitude and frequency of an AE event using fast Fourier transform

Figure 4 shows an AE signal acquired during the LMD process in the presence of defects; the spikes in the signal are events which have features different from the rest of the AE signal. The AE event is counted when the amplitude of the signal is higher than a preset threshold which is the background noise preceded and followed by a signal with amplitude lower than the threshold for a certain period.

Different defect mechanisms can produce a similar waveform and amplitude; it is not sufficient to use a particular feature to represent the events. Therefore, seven AE signal features (Table 3) were employed in the clustering analysis to overcome this problem. Representing the AE signal with enough features is critical to collect as much information as possible about the emitting source, especially when there is little literature regarding the use of AE technique in monitoring LMD process that can be used as a reference in AE feature selection. The AE signal can be represented in the frequency domain using fast Fourier transform (FFT) or in the time domain using peak amplitude, kurtosis, energy, the number of counts, duration, and rise time. Figure 5 shows some of the time-dependent features.

Among all the features, the signal amplitude alone was measured in real time by the data acquisition system. All the other descriptors were calculated from the

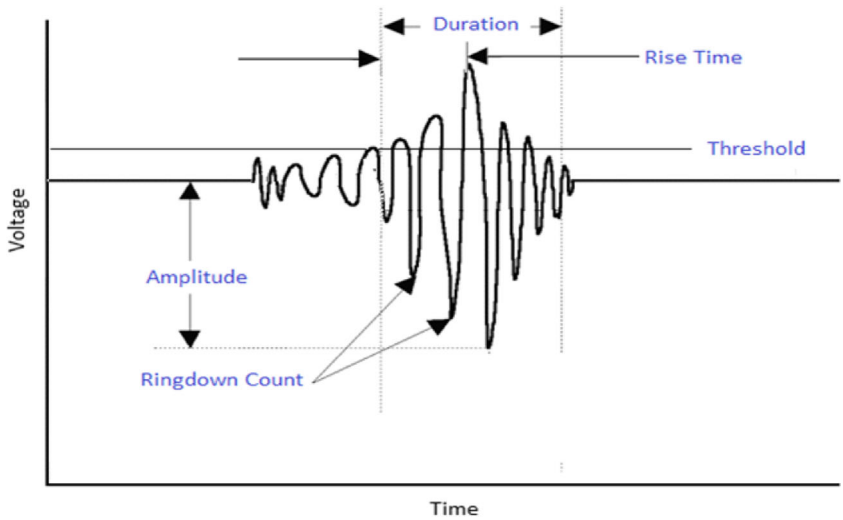

Fig. 5 Time-dependent AE event features

Table 4 Standardized of the AE signal features

Event number	Rise time	Peak amplitude	Duration	Kurtosis	Number of counts	Energy	Frequency
1	−0.8632828	−0.7341107	−0.68626	−1.44472	−0.75435274	−0.42589	−1.27045
2	−0.1261721	−0.6508765	−0.60598	−1.25783	−0.6648721	−0.42121	−0.28512
3	−0.6931803	−0.6231318	−0.62959	−0.34811	−0.6786384	−0.42337	−0.16714
4	−0.0694712	−0.5398975	−0.51153	−0.52405	−0.5478591	−0.41726	−0.57824
5	−0.2584740	−0.4844081	−0.55876	0.728254	−0.5960409	−0.4176	1.576003
6	−0.2962745	−0.5121528	−0.28959	−0.16773	−0.2174693	−0.41689	0.226959
7	−0.5797787	−0.5676423	−0.53514	0.00428	−0.5547422	−0.42265	0.843153
8	2.803370	2.0958524	2.3407	−1.1222	2.2535706	2.41352	0.053381
9	−0.1072718	−0.6786212	−0.53987	−0.14773	−0.5409760	−0.42517	1.349834
10	−0.5608784	−0.7063660	−0.64376	−1.04886	−0.6924046	−0.42553	−0.08978
11	−0.3151748	0.3201892	−0.02042	0.449555	−0.0109757	−0.31195	1.354937
12	−0.3340751	−0.4844081	−0.68626	1.881232	−0.7612358	−0.42228	−0.71316
13	2.1796615	2.0958524	1.953476	−0.93525	1.9231809	1.795566	−0.14501
14	−0.1828729	−0.5121528	−0.29903	0.510621	−0.2381187	−0.41256	0.799576
15	−0.5041776	−0.3734291	−0.33681	0.103122	−0.3138330	−0.40788	−0.4526
16	1.8583568	2.0958524	1.967643	−1.38266	1.7029210	2.668412	−0.04808
17	−0.1639726	−0.6231318	−0.23292	0.998504	−0.1142225	−0.42121	1.881284
18	0.0628306	0.9860629	0.267636	2.358211	0.3882451	−0.26322	0.568001
19	−0.8632828	−0.6786212	−0.74765	0.445735	−0.8438333	−0.42517	−0.77585
20	−0.7309809	−0.734110	−0.7382	−0.56879	−0.8300670	−0.42589	−0.82462
21	−0.5986790	0.1259761	−0.17625	0.437646	−0.1555213	−0.35378	−0.48302
22	−0.1828729	0.1814655	0.02208	0.054488	0.0785047	−0.33756	−0.34344
23	−0.5797787	−0.4566633	−0.1007	1.929897	−0.0109757	−0.38877	0.603812
24	−0.5608784	−0.234705	−0.28487	−0.16722	−0.2587681	−0.39165	1.376322
25	−0.0316707	0.1814655	−0.09598	1.216332	−0.0316251	−0.36316	−0.00579
26	−0.4852773	−0.6231318	−0.28487	−0.57514	−0.1761706	−0.42337	−0.00107
27	−0.2017732	−0.4566633	−0.41237	1.534873	−0.3620149	−0.4212	−2.1943
28	−0.4852773	−0.7063660	−0.51626	−0.96409	−0.5203266	−0.42445	−2.15717
29	0.0817309	−0.6786212	−0.42653	−1.13012	−0.3757811	−0.42517	1.515988
30	0.8755425	1.9293840	0.65486	1.466014	0.8218817	0.066326	−0.03145
31	2.7277695	2.0958524	2.760979	−1.11484	2.8042202	2.811349	−2.23613
32	−0.6931803	−0.734110	−0.69098	0.127625	−0.7612358	−0.42589	0.776849
33	−0.6931803	−0.7063660	−0.72403	0.144849	−0.8094177	−0.42553	0.102579
34	−0.5608784	−0.4566633	−0.23764	−0.33667	−0.1899369	−0.40212	0.40919
35	2.066259	2.0958524	2.765701	−1.07521	2.7835709	2.630087	−0.15449
36	−0.8632828	−0.6786212	−0.67209	−0.25692	−0.7337033	−0.42517	0.082367
37	−0.0694712	0.4311682	−0.04875	0.176898	−0.0109757	−0.2917	-0.56332

waveforms at the end of deposited layer because they are very dependent on the amplitude threshold used to detect the arrival time and the end of an AE signal. In this work, all these features were used in a multi-parameter statistical analysis and clustering analysis. No AE noise associated with the operation of the laser system or the CNC system were observed. Also, it was found in this study that the noise level is much smaller than the signals of interest. Also, a frequency filtering was used which allows the passing of only those signals falling within a selected bandwidth (100 kHz to 1 MHz).

Table 5 Eigenvalues of the seven AE signal features

Eigenvalue	4.9119	1.0895	0.8222	0.0826	0.0559	0.0377	0.0002
Proportion	0.702	0.156	0.117	0.012	0.008	0.005	0.000
Cumulative	0.702	0.857	0.975	0.987	0.995	1.000	1.000

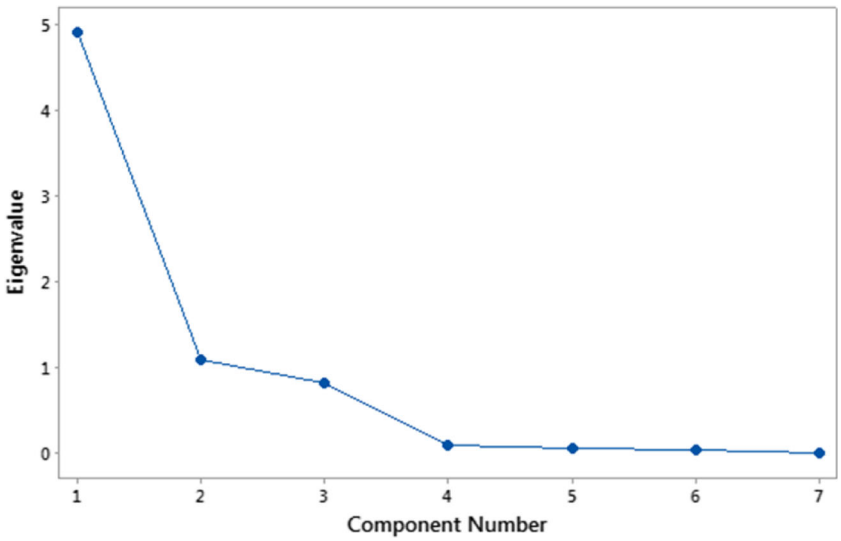

Fig. 6 Time-dependent AE event features

3 Results and discussion

3.1 Principal component analysis

Principal component analysis (PCA) was used here for the sake of dimensionality reduction, and the results of the clustering analysis cannot be visualized in their original dimension (seven-dimensional data set). PCA is a statistical technique which utilizes an orthogonal transformation to convert a set of correlated variables into a set of values linearly uncorrelated known as principal components. PCA is used to approximate the data matrix of features to reduce the number of related dimensions. This can be done by finding the directions that explain the maximum variation in the data set and then project into a subspace with lower dimensions. The seven features calculated from AE events are the components of the n input pattern vectors Z_i (i = 1, 2, …, n).

$$Z = \begin{bmatrix} z_1^t \\ z_2^t \\ \vdots \\ z_n^t \end{bmatrix} = \begin{bmatrix} z_1^1 & z_1^2 & \cdots & z_1^m \\ z_2^1 & z_2^2 & \cdots & z_n^m \\ \vdots & \vdots & \ddots & \vdots \\ z_n^1 & z_n^2 & \cdots & z_n^m \end{bmatrix} \tag{3}$$

where n is the number of events and m is the number of features. The data are first standardized by subtracting the mean from the dataset for each column then dividing by the column standard deviation (the mean is equal to zero, and the standard deviation is equal to one). Table 4 shows the standardization of the AE signal features.

Then covariance matrix can be calculated by

$$\mathrm{Cov}_Z = E\left[ZZ^T\right] \tag{4}$$

Z^T is the transpose matrix of matrix Z. The eigenvectors and corresponding eigenvalues were computed.

$$\mathrm{Cov}_Z\ \alpha = \beta\alpha \tag{5}$$

where α is the eigenvector and β is the eigenvalue for each principal component (see Table 2).

As the covariance matrix is a symmetric matrix and has an orthogonal basis, the data can be represented in terms of only a few basis vectors of the orthogonal basis in which the data set has the most significant amounts of variance (Table 5).

Table 6 Average silhouette width for different number of clusters

Number of clusters	Average silhouette width
2	0.8727
3	0.4201
4	0.4957
5	0.4902
6	0.4641
7	0.4949
8	0.4416
9	0.4163
10	0.4294
11	0.4117

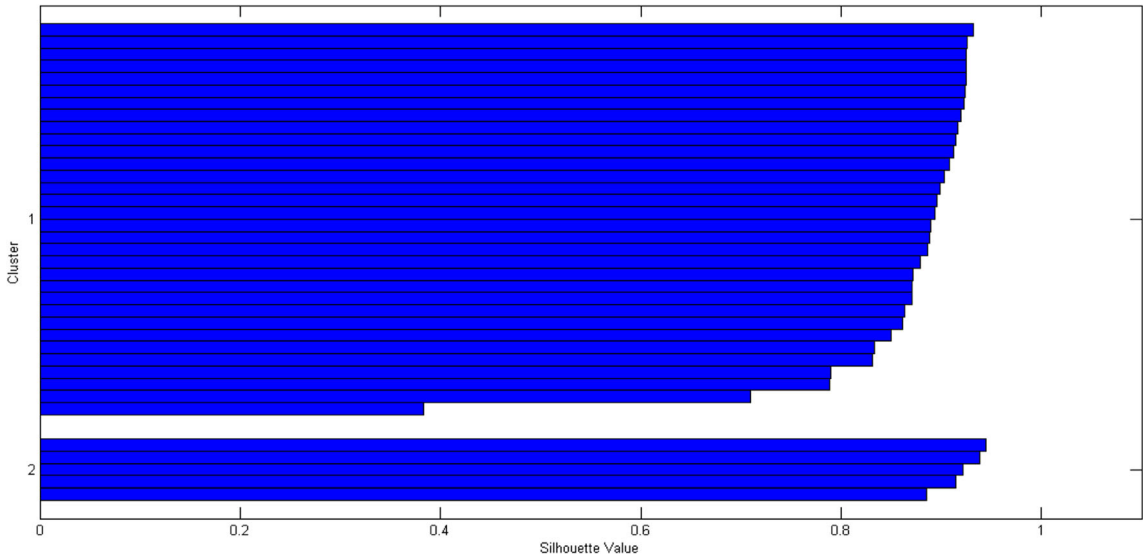

Fig. 7 Silhouette width value for the events in the two clusters

As can be seen in Fig. 6 and Table 5, the first two principal components are explaining 85.7 % of the variance, and these principal components will be used to reduce the dimension of the set of features from seven dimensions to just two dimensions for better visualization.

The k eigenvectors with the largest eigenvalues were chosen to construct eigenvector matrix Y_T. In the last step, the data was transformed onto the new subspace via the equation

$$W = Z\,Y_T \tag{6}$$

which represents the new coordinates of the n patterns in the orthogonal coordinate system defined by the eigenvectors. The reduced dimension will not be used in the clustering analysis to obtain the most accurate clustering results.

Table 7 Cluster centers

Feature	Cluster	
	1	2
Rise time (ms)	0.4513268	2.080529
Peak amplitude (V)	1.8124335	8.8001
Duration (ms)	1.636167	8.2521209
Kurtosis	6.7799735	3.6725249
Number of counts	132.29273	517.29255
Energy (dB)	615.14928	290,869.4423
Frequency (kHz)	25.098233	19.090999

3.2 Clustering analysis

It is not easy to discriminate precisely the AE signal associated with each defect source from the waveform of the signal; thus, it is useful to use clustering analysis. Clustering analysis is a machine learning technique which groups the AE events based on their features to create clusters in such a way that the AE events inside a cluster are similar to each other, and also dissimilar from events in other clusters. In this work, the K-means clustering algorithm was used to group the AE events into homogeneous subgroups (clusters). A silhouette width value was used to find the optimal number of clusters.

The K-means clustering algorithm aims to minimize within-cluster distances between all the vectors of a cluster and its center and maximize the distances between the centers of all clusters. The clustering algorithm requires the number of clusters k to be known and specified in advance; thus, the silhouette width was used for a range of clusters from two clusters to ten clusters. The number of clusters with the maximum average silhouette width was used to group the AE events into subgroups reflecting the number of defects. The K-means algorithm can then be described as follows:

1. Specify the maximum number of clusters (r).
2. Assume the number of clusters k from 1 to r and randomly initialize each cluster center C_i, where i is from 1 to k
3. Calculate the Euclidean distance between the vector and the centers of the clusters and then assign each input vector (or pattern) to the nearest cluster.

Table 8 Cluster membership

Event number	Cluster	Distance
1	1	2.263
2	1	1.581
3	1	0.838
4	1	1.054
5	1	1.635
6	1	0.453
7	1	0.886
8	2	0.814
9	1	1.404
10	1	1.378
11	1	1.538
12	1	1.956
13	2	0.830
14	1	0.847
15	1	0.559
16	2	1.041
17	1	2.032
18	1	2.805
19	1	1.248
20	1	1.425
21	1	0.851
22	1	0.910
23	1	1.899
24	1	1.366
25	1	1.281
26	1	0.844
27	1	2.657
28	1	2.551
29	1	2.024
30	1	3.287
31	2	1.930
32	1	1.015
33	1	0.764
34	1	0.688
35	2	0.783
36	1	0.891
37	1	1.139

4. Recalculate the location of the cluster center according to the nearest mean.
5. Repeat steps 2 and 3 until there are no changes in these center locations.
6. Calculate the maximum average silhouette width.
7. Repeat steps from 2 to 6 for all possible number of clusters.

The greater the silhouette value, the better the clustering results [19, 20]. The optimal value of k is determined according to the maximum of the silhouette width defined as

$$s(k) = \frac{1}{n}\sum_{l=1}^{n} \frac{\min(b(l,k) - a(l))}{\max(a(l), \min(b(l,k)))} \tag{7}$$

where $a(l)$ is the average distance between l-th event and all other events in the same cluster, and $b(l,k)$ is the minimum of the average distances between the l-th event and all the events in each other cluster. The silhouette width values range from −1 to 1. If the silhouette width value for an event is about zero, it means that the event could be assigned to another cluster. If the silhouette width value is close to −1, it means that the event needs to be assigned to another cluster. If the silhouette width values are close to 1, it means that the event is well clustered. A clustering can be evaluated by the average silhouette width $s(k)$ of individual events.

The largest average silhouette width, over different K, indicates the best number of clusters. As can be seen in Table 6, the greatest average silhouette width is 0.8727, which means that k = 2 is the optimum number of clusters. Figure 7 shows the silhouette width values for the individual AE events in clusters one and two; most of the silhouette width values are close to 1, which means that the AE events are well clustered.

Table 7 shows the final clusters centers; the final cluster centers are calculated as the mean for each feature within each final cluster, and the final cluster centers reveal the characteristics of each detected defect. The defects represented by cluster two tend to have more energy, longer duration, slower rise time, larger number of counts, higher amplitude, are close to the normal distribution with flatter and light tail distribution, and have less frequency compared to the defects which are represented by cluster one. Table 8 shows the cluster membership and the distance between each AE event and the center of the cluster. The size of cluster one is 32, which means 86.5 of the AE events; cluster two contains five AE events (15.5 % of the AE events).

Here, the principal component analysis (PCA) was used for dimensionality reduction to visualize the results of the clustering analysis. Even though the principal component analysis showed that two principal components are explaining 85.7 % of the variance, the third principal component was used for the better representation of the AE events; the distribution of the AE events between the two clusters can be seen in Fig. 8. It is worth mentioning that the second and the third principal

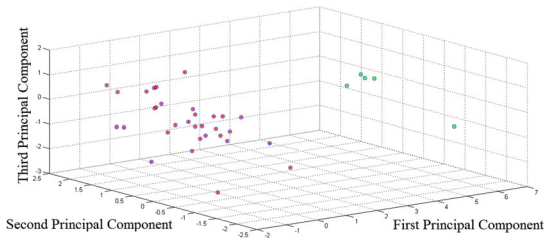

(a) Three Principal Components contain 97.5 % of Variance

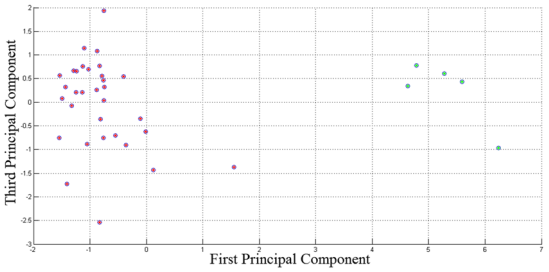

(b) First and Third Principal Components contain 81.9 % of Variance

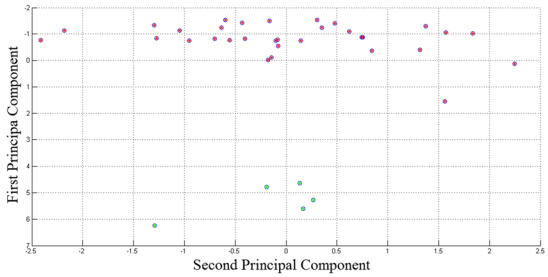

(c) First and Second Principal Component contain 85.7 % of Variance

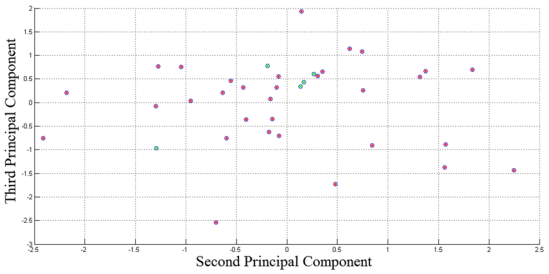

(d) Second and Third Principal Component contain 27.3 % of Variance

Fig. 8 **a–d** Principal component projection and clusters distribution for the AE events

components alone are poorly representing the cluster distribution since they only explain 27.3 % of the variance in the original data.

Table 9 presents the analysis of variance (ANOVA) of the cluster centers. As can be seen, most of the means of clustering features differ significantly across the two clusters because the null hypothesis (means are equal) is rejected in a case at significance level ≤0.05. The frequency is not significant, which means that it has little contribution to the cluster solution. The features with large F value provide the greatest separation between clusters. As the F value increases, the importance of feature increases; this is also illustrated in Fig. 9. The dissimilarities in the events features between the two types of clusters lead to the conclusion that the AE source mechanisms are not the same in both clusters.

3.3 Defects types and optical microscopy study

After preparing the surface of deposited metal, the cracks and pores were observed using an optical microscope; the number of cracks to the number of pores strongly

Table 9 Analysis of variance (ANOVA) of the cluster centers and features importance

	Cluster		Error		F	Significance	Importance
	Mean square	df	Mean square	df			
Rise time	31.307	1	0.134	35	233.503	0.000	3
Peak amplitude	25.395	1	0.303	35	83.809	0.000	5
Duration	32.137	1	0.110	35	291.130	0.000	2
Kurtosis	7.330	1	0.819	35	8.949	0.005	6
Number of counts	30.410	1	0.160	35	190.403	0.000	4
Energy	35.369	1	0.018	35	1960.776	0.000	1
Frequency	1.481	1	0.986	35	1.501	0.229	7

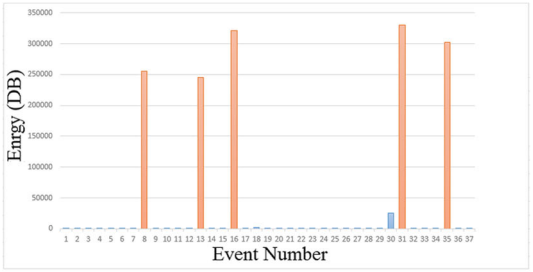

(a) Events in cluster one have less energy

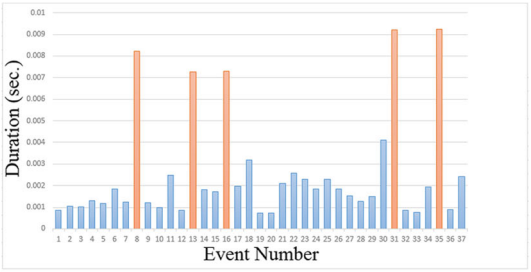

(b) Events in cluster one have shorter duration

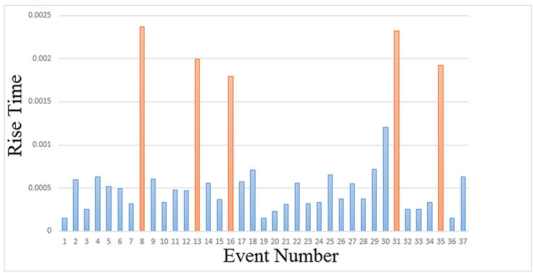

(c) Events in cluster one have faster rise time

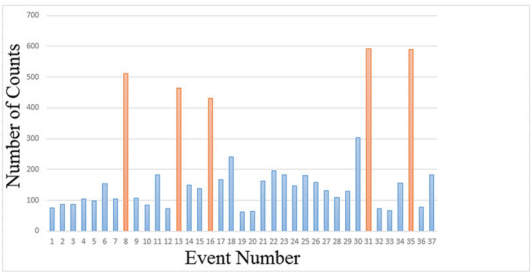

(d) Events in cluster one have less number of counts

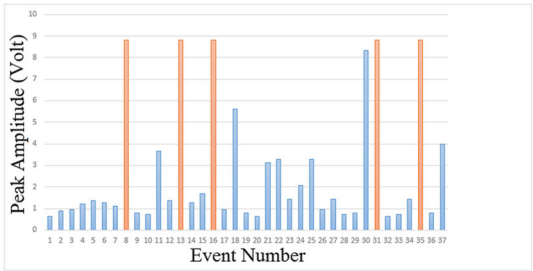

(e) Events in cluster one have smaller amplitude

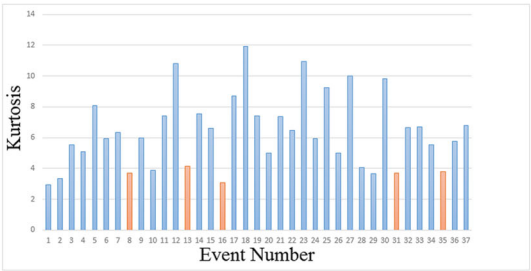

(f) Events in cluster one is peaked distribution

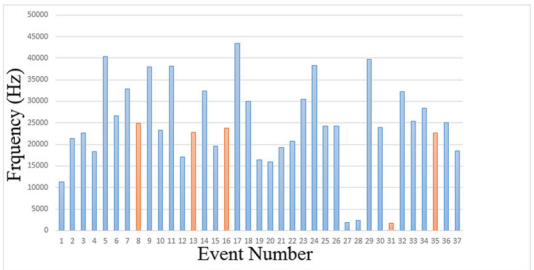

(g) Events in cluster one have larger frequency

Fig. 9 **a**–**g** Comparing the features of the AE events in clusters one and two

correlated with the number of events in cluster two to the number of events in cluster one. Also from the literature [10, 22], the waveform and the features of the acoustic emission signal created by cracks is similar to the events in cluster two.

The first type of observed defects is pores that have a spherical form and appear in random locations not associated with the microstructure as shown in Fig. 10a. The possible sources of these porosities are surface powder contamination [21], gases trapped within the powder particles due to the difference in the powder sizes, and an oxidation effect since the oxygen level was high because the chamber was not used to stimulate defect formation in this research. In fact, surface oxides may most likely remain in the solid state in the melting pool and, as such, upset the wetting mechanisms that melted the powder and induce voids. The waveform from cluster one (Fig. 10b) is quite different

(a) Optical Image of Gas Porosity

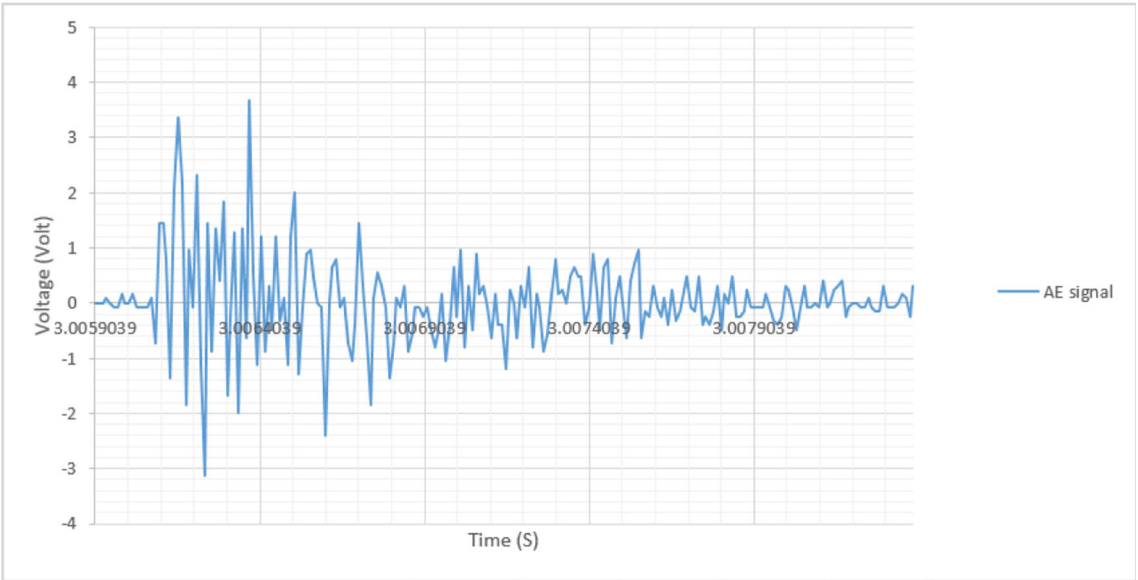

(b) Sample of Waveform Signal from Cluster One

Fig. 10 **a**, **b** Optical image of a transverse cross-sectioned laser deposit showing a gas porosity and a waveform sample from cluster one

from the waveform from cluster two (Fig. 11b), with shorter decay time and less amplitude.

Figure 11a displays a crack caused by thermal stress. The temperature gradient of the deposited layer is large in the direction of thickness during laser deposition process, and the thermal expansion coefficients of the two deposition materials are different, which results in the thermal stress at the combining surface of deposition, thus the cracks are formed. It also occurs with powder contamination in the powder feeder [21]. The waveform from cluster one is quite different from the waveform from cluster two, with shorter decay time and less amplitude.

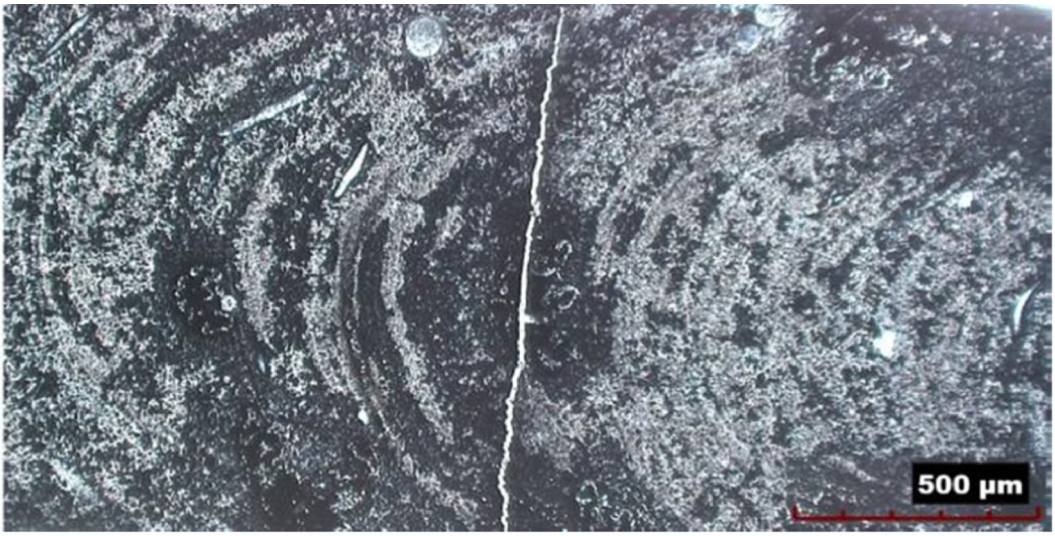

(a) Optical Image of Showing a Crack

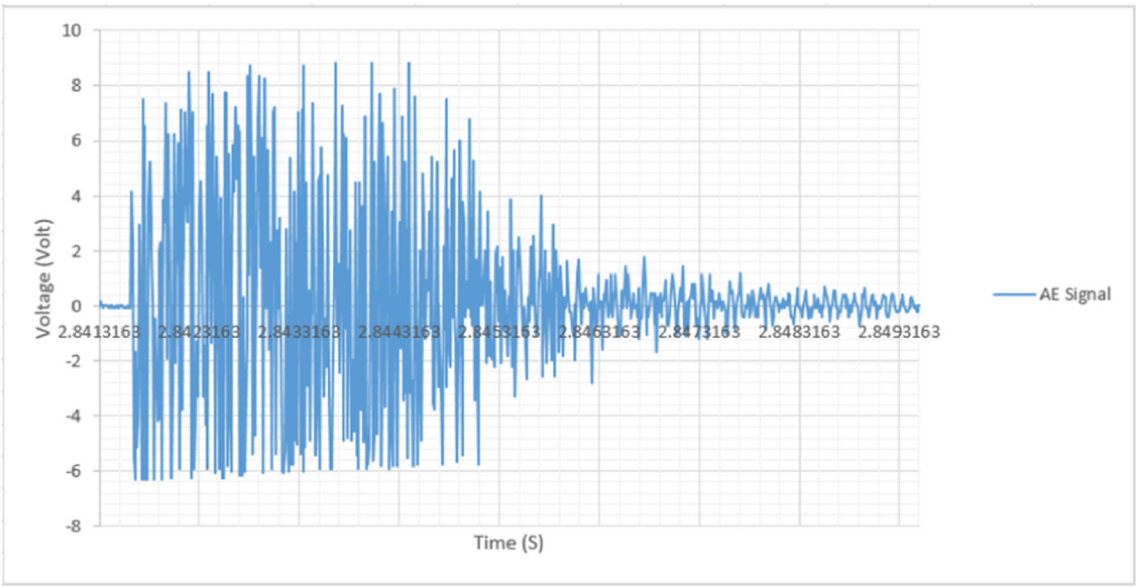

(b) Sample of Waveform Signal from Cluster Two

Fig. 11 **a**, **b** Optical image of a transverse cross-sectioned laser deposit showing a crack and a waveform sample from cluster two

4 Conclusions

The AE signal was collected during the LMD in an oxidized environment with mixed metal powders to stimulate all possible types of defects. Several defects mechanisms were activated and detected by the AE sensor. K-Means clustering method was implemented to analyze the AE signals and identify defect source mechanisms. Principal components analysis was used to facilitate the visualization of the clusters in 2D and 3D plots.

The clustering results successfully distinguish two main defects types and their signal characteristics. The number of clusters to be created does not have to be specified in advance; they only depend on the number of defects being created. Porosities produce the AE signals with shorter decay time and less amplitude. The cracks trigger the AE signals with short durations and high amplitudes. The signal energy is a crucial feature in identifying the AE defect source mechanisms.

The validation of the proposed methodology has been carried out using an optical microscope; it showed the correlation between the number of acoustic events and the number of defects determined by post-test optical microscopy. The numbers of signal events in each cluster are

in agreement with the rough estimations of the associated numbers of defects.

Acknowledgments This research was supported by the National Science Foundation grants IIP-1345240, CMMI-1301414, and CMMI-1547042. Support from Product Innovation and Engineering, LLC, Missouri S&T Intelligent Systems Center, and the Missouri S&T Manufacturing Engineering Program is also greatly appreciated.

References

1. Wang L, Felicelli SD, Craig JE (2009) Experimental and numerical study of the LENS rapid fabrication process. ASME J Manuf Sci Eng 131(4):041019–041019-8. doi:10.1115/1.3173952
2. V. Weerasinghe, W. Steen (1983) Laser cladding by powder injection. In: Proc. 1st Int. Conf. Lasers Manuf., p 125–132
3. Weerasinghe V, Steen W (1987) Laser cladding with blown powder. Met Constr 19:581–585
4. Sears J (1999) Direct laser powder deposition—'State of the Art', No. KAPL-P-000311; K99089, Knolls At. Power Lab., Nis. NY
5. McLean M (1997) Laser direct casting high nickel alloy components. Adv Powder Metall Part Mater 3:21
6. Mazumder J, Choi J, Nagarathnam J, Koch K, Hetzner D (1997) The direct metal deposition of H13 tool steel for 3D components. JOM 49:55–60
7. Lewis G, Nemec R, Milewski J, Thoma D (1994) Directed light fabrication, No. LAUR-94-2845; CONF-9410189-2, Los Alamos Natl. Lab., NM, USA
8. Milewski J, Lewis G, Thoma D (1998) Directed light fabrication of a solid metal hemisphere using 5-axis powder deposition. J Mater Process Technol 75:165–172
9. Wu X, Liang J, Mei J, Mitchell C, Goodwin PS, Voice W (2004) Microstructures of laser-deposited Ti-6Al-4V. Mater Des 25:137–144
10. Arcella F, Froes F (2000) Producing titanium aerospace components from powder using laser forming. JOM 52:28–30
11. J. Fessler, R. Merz, Laser deposition of metals for shape deposition manufacturing, In: Proc Solid Free Fabr Symp, Univ Texas, Austin, 1996, pp. 117–124.
12. Keicher DM, Miller WD (1998) LENS moves beyond RP to direct fabrication. Met Powder Rep 53:26–28
13. Griffith M, Schlienger M, Harwell L (1998) Thermal behavior in the LENS process, No. SAND-98-1850C; CONF-980826-, Sandia Natl. Labs, Albuquerque, NM, USA
14. Xue L, Islam M (1998) Free-form laser consolidation for producing functional metallic components. Laser Inst. Am. Laser Mater Process 84
15. Xue L, Islam M (2000) Free-form laser consolidation for producing metallurgically sound and functional components. J Laser Appl 12: 160–165
16. Ma Z, Sun G, Liu D, Xing X (2016) Dissipativity analysis for discrete-time fuzzy neural networks with leakage and time-varying delays. Neurocomputing 175 :579–584Part A
17. Liao Z, Axinte DA (2016) On monitoring chip formation, penetration depth and cutting malfunctions in bone micro-drilling via acoustic emission. J Mater Process Technol 229:82–93
18. Gaja H, Liou F (2016) Automatic detection of depth of cut during end milling operation using acoustic emission sensor. Int J Adv Manuf Technol
19. Gutkin R, Green CJ, Vangrattanachai S, Pinho ST, Robinson P, Curtis PT (2011) On acoustic emission for failure investigation in CFRP: pattern recognition and peak frequency analyses. Mech Syst Signal Process 25(4):1393–1407
20. Rousseeuw PJ (1987) Silhouettes: a graphical aid to the interpretation and validation of cluster analysis. J Comput Appl Math 20:53–65
21. Barua S et al. ((2014)) Vision-based defect detection in laser metal deposition process. Rapid Prototyp J 20(1):77–85
22. Lu SP et al. (2003) Acoustic emission monitoring and microscopic investigation of cracks in ERCuNi cladding. J Mater Sci Technol 19(3):201–205